GPU-Accelerated Parallel Bilevel Optimization for Robust 6G ISAC

Xingdi Chen, Kai Yang*

School of Computer Science and Technology, Tongji University, China
xingdichen@tongji.edu.cn, kaiyang@tongji.edu.cn

Abstract

This paper initiates the first exploratory study to investigate the robust integrated sensing and communication (ISAC) systems under channel estimation errors from the perspective of GPU-accelerated bilevel optimization. Within this framework, the upper-level problem is dedicated to simultaneously optimizing communication and sensing objectives, quantified respectively by weighted sum rate and Cramér-Rao lower bound, while the lower-level problem considers the channel uncertainties. We then propose an efficient algorithm that can find a set of Pareto optimal solutions with different trade-offs among communication rates and sensing accuracy. The theoretical analysis regarding the convergence rate has also been provided. Furthermore, we design a bilevel optimization inspired deep neural network architecture for that can be realized efficiently on GPU platform. Experiments have been conducted to evaluate the performances of proposed methods. In particular, the proposed GPU-accelerated parallel bilevel optimization can accelerate the convergence speed by up to 50 times compared to conventional gradient-based methods. This characteristic renders it especially suitable for real-time applications, exemplified by the demanding requirements of robust ISAC in upcoming 6G networks.

Introduction

Recently, bilevel optimization has gained significant interest in machine learning, with applications in various areas like hyperparameter optimization (Liu et al. 2021; Franceschi et al. 2018), meta-learning (Ji et al. 2020; Ji, Yang, and Liang 2021) and neural architecture search (Liu, Simonyan, and Yang 2018; Xue et al. 2021). Bi-objective optimization research is a crucial component of the multi-objective optimization, which has also achieved significant success in multi-task learning (Chen and Kwok 2022a,b; Lin et al. 2019). Multi-objective bilevel optimization can be applied to robust meta-learning, robust neural architecture search, and multi-task learning(YE et al. 2021; Ye et al. 2024).

However, bi-objective bilevel optimization is under-explored, with only a handful of related studies (Gutjahr and Dzubur 2016; Camacho-Vallejo et al. 2022). The bi-objective bilevel optimization problem can be formulated as

$$\begin{aligned} \min_{\boldsymbol{x}} \quad & [F_1(\boldsymbol{x},\boldsymbol{y}), F_2(\boldsymbol{x},\boldsymbol{y})]^T \\ \text{s.t.} \quad & G(\boldsymbol{x},\boldsymbol{y}) \leq 0 \\ & \boldsymbol{y} \in \arg\min_{\boldsymbol{y}'} \quad [f_1(\boldsymbol{x},\boldsymbol{y}'), f_2(\boldsymbol{x},\boldsymbol{y}')]^T \\ & \qquad \text{s.t.} \quad g(\boldsymbol{x},\boldsymbol{y}') \leq 0, \end{aligned} \tag{1}$$

where $\boldsymbol{x} \in \mathbb{R}^{n_1}$ and $\boldsymbol{y} \in \mathbb{R}^{n_2}$ are the upper-level and lower-level variables, respectively. Both upper-level and lower-level objectives are vector-valued. We refer to G as the upper-level constraint and g as the lower-level constraint. Apparently, robust optimization, characterized by a max-min or min-max structure, is fundamentally a bilevel optimization problem.

Integrated sensing and communication (ISAC), a revolutionary technology for future sixth-generation (6G) wireless networks, has received significant attention recently. Unlike conventional wireless networks with communication functionality only, ISAC seamlessly integrates both communication and sensing, paving the way for numerous environment- and location-aware applications such as autonomous driving, smart city, and factory automation (Liu et al. 2022a; Zhang et al. 2022b). Beamforming, one of the most promising multi-antenna techniques, can shape transmit signals in specified directions, playing a crucial role in enhancing the system performance of ISAC. Extensive studies on beamforming design have been proposed to provide high-quality communication and sensing services (Hua, Xu, and Han 2023; Liu et al. 2022b, 2020; Cheng et al. 2024; Xu et al. 2023).

However, most prior works on beamforming design for ISAC assume the knowledge of channel state information (CSI) at base stations (BSs) is perfectly known. Unfortunately, CSI errors, which can have catastrophic effects on the performance of both communication and sensing (Wang et al. 2024), are inevitable due to the following three reasons (Tajer, Prasad, and Wang 2011). Firstly, channel estimation based on statistical methods cannot provide accurate channel estimates when training samples are limited, which is referred to as estimation error. Secondly, the amount of bits reserved for quantized CSI feedback is small in future wireless networks, leading to what is known as quantization error. Thirdly, the communication channel is time-varying.

*Corresponding author.

On the other hand, existing research on ISAC typically relaxes beamforming design problems into semidefinite programming (SDP) which is very time-consuming to solve.

To address above problems, we consider a networked ISAC system considering bounded CSI errors in this paper. The weighted sum rate (WSR) and Cramér-Rao lower bound (CRLB) are employed as performance metrics for communication and localization estimation, respectively. Communication and localization performance are conflicting objectives under limited resources, making the problem suitable for bi-objective optimization. Building upon this, when incorporating CSI errors, the problem can be formulated as a bi-objective bilevel optimization problem. Inspired by (Lin et al. 2019; Fliege and Svaiter 2000; Jiao et al. 2023, 2024; Yang et al. 2008, 2014), we propose a **B**i-**O**bjective **BiL**evel optimization based **R**obust **B**eam**F**orming (BOBLRBF) algorithm to tackle this challenging strongly non-convex problem. To be specific, the bi-objective bilevel optimization problem is divided into several subproblems with different preference vectors. Following this, we regard the lower-level optimization problem as a constraint to the upper-level optimization problem and utilize cutting planes to approximate this constraint. These subproblems are solvable in parallel, enabling the algorithm to yield a collection of well-distributed Pareto critical solutions.

Deep neural networks (DNNs) provide unprecedented performance gains in many real world problems. Wu et al. (2024) points out that DNNs designed using convergent first-order optimization algorithms with bounded width can be universal approximators under mild conditions. Therefore, we design a BOBLRBF inspired neural network architecture called BOBLRBF-DNN, where the forward pass is interpreted as the updates of the optimization algorithm. The designed DNN can learn the gradient information of iterative algorithms. This method can handle batch samples, unlike BOBLRBF, which can only solve one sample at a time. Benefiting from the parallel computing capabilities of GPUs, this method converges faster compared to the BOBLRBF algorithm, making it more suitable for large-scale ISAC systems.

The main contributions of this paper are:

- This is the first work that proposes a robust beamforming design framework for ISAC systems employing bi-objective bilevel optimization. Unlike prior studies that assume perfect CSI, we take CSI errors into account. This general framework can be readily adapted to other robust design problems within ISAC systems.
- An iterative algorithm, named BOBLRBF, is proposed to tackle this challenging non-convex problem with hierarchical dependencies. The algorithm can generate well-distributed Pareto critical solutions with different trade-offs among communication and sensing for practitioners to choose from. Moreover, a theoretical analysis regarding the iteration complexity has also been provided.
- We propose a GPU-accelerated bilevel optimization architecture called BOBLRBF-DNN, which is inspired by the convergent algorithm BOBLRBF. This method is scalable, which means that as the number of GPUs increases or computing capability improves, the algorithm converges faster, rendering it particularly suitable for real-time applications where rapid convergence is essential.

Related Work

Bi-Objective Bilevel Optimization. The mainstream methods for solving bilevel optimization problems are predominantly based on gradient approaches (Liu et al. 2021; Hong et al. 2023). Several methods are commonly used for bi-objective optimization problems, including the weighted sum, ε-constraint method, and hybrid method (Kim and De Weck 2005; Yeung and Zhang 2023). However, bi-objective bilevel optimization is under-explored (Gutjahr and Dzubur 2016; Camacho-Vallejo et al. 2022). To the best of our knowledge, the bi-objective bilevel optimization approach has not yet been applied in ISAC systems.

Accelerated Bilevel Optimization. Unrolling is a promising technique that has established a connection between iterative algorithms, such as those used in sparse coding, and neural network architectures (Gregor and LeCun 2010). Typically, the designer begins with an optimization problem with an explicit objective function, and DNNs are then derived by unrolling the iterative process that solves the problem. However, prior research has primarily focused on unrolling for single-level optimization problems (Yang et al. 2020; Li et al. 2019; Adler and Öktem 2018). We are the first to explore GPU-accelerated bilevel optimization, which can enhance convergence speed by up to 50 times compared to traditional iterative methods.

Integrated Sensing and Communication. Conventionally, mono-static ISAC systems where a single BS serves as an ISAC transceiver, and bi-static ISAC systems in which two BSs are deployed as the ISAC transmitter and sensing receiver, respectively, have been widely investigated (Hua, Xu, and Han 2023; Liu et al. 2022b, 2020; Zhang et al. 2022a; Liu et al. 2018; Cao et al. 2020; Chen and Gu 2021). However, the mono-static and bi-static ISAC systems can only offer limited service coverage. To address the problem, networked ISAC systems have drawn significant research attention (Cheng et al. 2024; Xu et al. 2023; Huang et al. 2022; Wang et al. 2021; Demirhan and Alkhateeb 2023).

Notations: $\mathbb{R}^{n\times m}$ and $\mathbb{C}^{n\times m}$ are used for the sets of n-by-m dimensional real matrices and complex matrices, respectively. The notation $\boldsymbol{x} \sim \mathcal{CN}(\bar{\boldsymbol{x}}, \boldsymbol{\Sigma}_{\boldsymbol{x}})$ indicates that $\boldsymbol{x}$ is complex Gaussian distributed with mean $\bar{\boldsymbol{x}}$ and covariance $\boldsymbol{\Sigma}_{\boldsymbol{x}}$. We use $\Re(\cdot)$ and $\Im(\cdot)$ to denote the real and imaginary parts of the argument. The superscripts $(\cdot)^T$, $(\cdot)^H$ represent the transpose, conjugate transpose operations, respectively. Vec$(\boldsymbol{X})$ denotes the vector obtained by stacking the columns of matrix $\boldsymbol{X}$.

System Model

We consider a networked ISAC system as shown in Figure 1, consisting of J sensing targets of interest, L BSs indexed by $\mathcal{L} = \{1, 2, ..., L\}$, K_l single-antenna users in each cell associated with BS l indexed by $\mathcal{K}_l = \{1, 2, ..., K_l\}$. Let

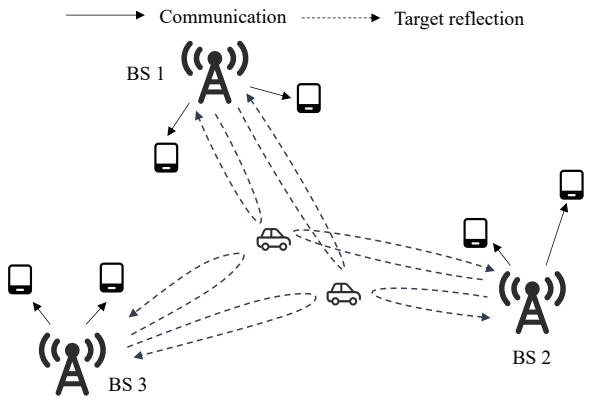

Figure 1: An illustration of the considered networked ISAC system comprising $J = 2$ sensing targets of interest, $L = 3$ BSs, each associated with $K_l = 2$ users.

$\mathrm{U}_{l,i}$ denote the i-th user associated with BS l. In this system, BSs send messages and dedicated sensing signals to their associated users, and the echo signals reflected from targets are collected by all BSs for target localization.

Let $s_{l,i}[t] \sim \mathcal{CN}(0,1)$ denote the communication signal for $\mathrm{U}_{l,i}$ and $\boldsymbol{s}_{l,0}[t] \in \mathbb{C}^{N\times 1}$ the dedicated sensing signal at the t-th time slot. In the time slot $t \in \mathcal{T} = \{1,2,...,T\}$, the transmitted signal from l is given by

$$\boldsymbol{s}_l[t] = \sum_{i\in\mathcal{K}_l} \boldsymbol{v}_{l,i} s_{l,i}[t] + \boldsymbol{s}_{l,0}[t], \tag{2}$$

where $\boldsymbol{v}_{l,i} \in \mathbb{C}^{N\times 1}$ represents the beamforming vector utilized for precoding the signal $s_{l,i}[t]$ before transmission, and we assume $\mathbb{E}[|s_{l,i}|^2] = 1$. Suppose the maximum transmit power budget at BS l is P_l, we have following constraints:

$$\sum_{i\in\mathcal{K}_l} ||\boldsymbol{v}_{l,i}||^2 + \mathrm{Tr}(\boldsymbol{Q}_{l,0}) \le P_l, \quad \forall l \in \mathcal{L}, \tag{3}$$

where $\boldsymbol{Q}_{l,0} = \mathbb{E}[\boldsymbol{s}_{l,0}[t]\boldsymbol{s}_{l,0}^H[t]] = \frac{1}{T}\sum_{t\in\mathcal{T}} \boldsymbol{s}_{l,0}[t]\boldsymbol{s}_{l,0}^H[t]$ denotes the sample covariance matrix of the sensing signal.

Communication Model

Let $\boldsymbol{h}_{l,c,k} \in \mathbb{C}^{N\times 1}$ denote the channel vector from BS l to $\mathrm{U}_{c,k}$ and $z_{c,k}[t] \sim \mathcal{CN}(0,\sigma_{c,k}^2)$ represent the additive complex white Gaussian noise at $\mathrm{U}_{c,k}$. The user $\mathrm{U}_{c,k}$ suffers from both the intra-cell and inter-cell interference, as well as the interference from the dedicated sensing signals. The power of each type of interference can be respectively expressed as follows

$$\begin{aligned} P_{\text{intra-cell}} &= \sum_{i\in\mathcal{K}_c, i\neq k} |\boldsymbol{h}_{c,c,k}^H \boldsymbol{v}_{c,i}|^2, \\ P_{\text{inter-cell}} &= \sum_{l\in\mathcal{L}, l\neq c} \sum_{i\in\mathcal{K}_l} |\boldsymbol{h}_{l,c,k}^H \boldsymbol{v}_{l,i}|^2, \\ P_{\text{sensing}} &= \sum_{l\in\mathcal{L}} \boldsymbol{h}_{l,c,k}^H \boldsymbol{Q}_{l,0} \boldsymbol{h}_{l,c,k}. \end{aligned} \tag{4}$$

Therefore, the SINR of $\mathrm{U}_{c,k}$ is given by

$$\mathrm{SINR}_{c,k} = \frac{|\boldsymbol{h}_{c,c,k}^H \boldsymbol{v}_{c,k}|^2}{P_{\text{intra-cell}} + P_{\text{inter-cell}} + P_{\text{sensing}} + \sigma_{c,k}^2}. \tag{5}$$

Considering CSI errors, we denote the imperfect CSI available at BSs by $\{\widetilde{\boldsymbol{h}}_{l,c,k}\}$ and define the channel estimation errors, which are unknown to BSs, as follows

$$\boldsymbol{\Delta}_{l,c,k} = \boldsymbol{h}_{l,c,k} - \widetilde{\boldsymbol{h}}_{l,c,k}, \quad \forall l,c,k. \tag{6}$$

We assume that such channel estimation errors are bounded and confined within an origin-centered hyper-spherical region of radius $\epsilon_{l,c,k}$, i.e., $\|\boldsymbol{\Delta}_{l,c,k}\|_2 \le \epsilon_{l,c,k}$. Therefore, the weighted sum rate can be defined as

$$\begin{aligned} &\mathrm{WSR}(\{\boldsymbol{v}_{l,i}, \boldsymbol{Q}_{l,0}, \boldsymbol{\Delta}_{l,c,k}\}) \\ &= \textstyle\sum_{c\in\mathcal{L}} \sum_{k\in\mathcal{K}_c} \alpha_{c,k} \log\left(1 + \mathrm{SINR}_{c,k}\right), \end{aligned} \tag{7}$$

where $\alpha_{c,k} > 0$ is the weighting factor corresponding to the user $\mathrm{U}_{c,k}$.

Sensing Model

In this subsection, we consider the distributed multi-target localization, in which the communication signals $\{s_{l,i}\}$ and dedicated sensing signals $\{\boldsymbol{s}_{l,0}\}$ are reused. Let $\mathcal{J} = \{1,2,...,J\}$ denote the set of targets at location $\boldsymbol{p} = [\boldsymbol{p}_1^T,...,\boldsymbol{p}_J^T]^T$ where $\boldsymbol{p}_j = [p_{j1}, p_{j2}]^T$ is the location of the jth target. Let $\boldsymbol{H}_{l,j,m} = \boldsymbol{a}(\theta_{r,j,m})\boldsymbol{a}^H(\theta_{t,j,l})$ denote the target response matrix where $\boldsymbol{a}(\theta)$ represents the steering vector. $\theta_{r,j,m}$ is the angle of arrival between the j-th target and the receiver $m \in \mathcal{L}$, and $\theta_{t,j,l}$ is the angle of departure between the BS $l \in \mathcal{L}$ and the j-th target. Then, the echo signal received by the receiver m can be expressed as

$$\boldsymbol{r}_m[t] = \sum_{l\in\mathcal{L}} \sum_{j\in\mathcal{J}} \alpha_{l,j,m} \boldsymbol{H}_{l,j,m} \boldsymbol{s}_l[t - \tau_{l,j,m}] + \boldsymbol{z}_{r,m}[t], \tag{8}$$

where $z_{r,m} \sim \mathcal{CN}(0,\sigma_{r,m}^2)$ represents the noise at the receiver m. $\alpha_{l,j,m}$ is the reflection coefficient incorporating both the radar cross section (RCS) and the path loss of the link from BS l to jth target and then to the receiver m. $\tau_{l,j,m}$ is the propagation time of a signal transmitted by BS l, reflected from target j, and received by the receiver m.

CRLB for Multi-Target Localization

According to information theory, CRLB provides a lower bound for the mean square error (MSE) on parameter estimation through an unbiased estimator. It is demonstrated in (Godrich, Haimovich, and Blum 2010) that the MSE of a maximum likelihood estimator is asymptotically tight to the CRLB at high SNR (over 10 dB). Thus, we derive the closed-form CRLB for multi-target localization in this section, expressed as a function of the beamforming vectors and sensing signals.

We introduce $\boldsymbol{R}_m = [\boldsymbol{r}_m[1],...,\boldsymbol{r}_m[T]] \in \mathbb{C}^{N\times T}$ as the matrix representation of received echo signals at the receiver m, given by

$$\boldsymbol{R}_m = \sum_{l\in\mathcal{L}} \sum_{j\in\mathcal{J}} \alpha_{l,j,m} \boldsymbol{H}_{l,j,m} \boldsymbol{S}_{l,j,m} + \boldsymbol{Z}_{r,m}, \tag{9}$$

where $\boldsymbol{S}_{l,j,m} = [\boldsymbol{s}_l[1-\tau_{l,j,m}],...,\boldsymbol{s}_l[T-\tau_{l,j,m}]] \in \mathbb{C}^{N\times T}$ and $\boldsymbol{Z}_{r,m} = [\boldsymbol{z}_{r,m}[1],...,\boldsymbol{z}_{r,m}[T]] \in \mathbb{C}^{N\times T}$. We define $\boldsymbol{\alpha}_{j,re} = [\Re(\alpha_{1,j,m}),...,\Re(\alpha_{L,j,m})]^T$ and $\boldsymbol{\alpha}_{j,im} =$

$[\Im(\alpha_{1,j,m}), ..., \Im(\alpha_{L,j,m})]^T$. The unknown parameters to be estimated are denoted by $\boldsymbol{\xi} = [\boldsymbol{p}^T, \boldsymbol{\alpha}^T]^T$, where $\boldsymbol{\alpha} \in \mathbb{R}^{2JL}$ is given by $\boldsymbol{\alpha} = [\boldsymbol{\alpha}_{1,re}^T, ..., \boldsymbol{\alpha}_{J,re}^T, \boldsymbol{\alpha}_{1,im}^T, ..., \boldsymbol{\alpha}_{J,im}^T]^T$. Let $\hat{\boldsymbol{\xi}}$ denote an estimate of the parameter $\boldsymbol{\xi}$ based on the observation $\{\boldsymbol{R}_m\}_{m=1,...,L}$.

Given that $\{s_{l,i}[t]\}$ and $\{\boldsymbol{s}_{l,0}[t]\}$ are independent over different users and times, and $\boldsymbol{H}_{l,j,m}, \forall l, j, m$, are independent, we can derive the CRLB for estimating the locations of targets $\boldsymbol{p}$ as follows

$$\begin{aligned} &\text{CRLB}(\{\boldsymbol{v}_{l,i}, \boldsymbol{Q}_{l,0}\}) \\ &= \text{Tr}\left((\boldsymbol{F}'_{\boldsymbol{pp}} - \boldsymbol{F}'_{\boldsymbol{p\alpha}}(\boldsymbol{F}'_{\boldsymbol{\alpha\alpha}})^{-1}(\boldsymbol{F}'_{\boldsymbol{p\alpha}})^T)^{-1}\right), \end{aligned} \tag{10}$$

where $\boldsymbol{F}'_{\boldsymbol{pp}} \in \mathbb{R}^{2J\times 2J}$, $\boldsymbol{F}'_{\boldsymbol{p\alpha}} \in \mathbb{R}^{2J\times 2JL}$ and $\boldsymbol{F}'_{\boldsymbol{\alpha\alpha}} \in \mathbb{R}^{2JL\times 2JL}$ are sub-matrices of the Fisher information matrix (FIM) $\boldsymbol{F}'_{\boldsymbol{\xi}}$ calculated in Appendix C for the parameter $\boldsymbol{\xi}$.

Problem Formulation and Method

In this section, we utilize the bi-objective bilevel optimization framework for the design of robust ISAC systems. Then, we develop an efficient algorithm based on cutting plane and steepest descent methods to generate a set of well-distributed Pareto critical solutions with different trade-offs among communication and sensing.

Problem Formulation

In the framework of bi-objective bilevel optimization, the upper-level problem is employed to model communication and sensing objectives, while the lower-level problem considers the robustness of the ISAC system. For notational simplicity, we split $\{\boldsymbol{v}_{l,i}, \boldsymbol{Q}_{l,0}\}$ into real and imaginary components and stack them into one vector denoted by $\boldsymbol{\gamma}$. $\boldsymbol{\delta}$ is defined in the same way. Then, the problem of optimizing the coordinated transmit beamforming to simultaneously maximize WSR and minimize CRLB in the presence of bounded CSI errors can be formulated as

$$\begin{aligned} \min_{\boldsymbol{\gamma}} \quad & [-\text{WSR}(\boldsymbol{\gamma}, \boldsymbol{\delta}), \text{CRLB}(\boldsymbol{\gamma})]^T \\ \text{s.t.} \quad & \textstyle\sum_{i\in\mathcal{K}_l} ||\boldsymbol{v}_{l,i}||^2 + \text{Tr}(\boldsymbol{Q}_{l,0}) \le P_l, \quad \forall l \\ & \boldsymbol{\delta} = \arg\min_{\boldsymbol{\delta}'} \text{WSR}(\boldsymbol{\gamma}, \boldsymbol{\delta}') \\ & \quad \text{s.t.} \quad \|\boldsymbol{\Delta}'_{l,c,k}\|_2 \le \epsilon_{l,c,k}, \quad \forall l, c, k. \end{aligned} \tag{11}$$

Problem (11) with two objectives at the upper level and one objective at the lower level is a special form of the bi-objective bilevel optimization problem. This framework can be readily extended to other robust ISAC system designs. More insights into problem (11) are provided in Appendix B.1.

Method: BOBLRBF

We aim to generate a set of well-distributed solutions with different trade-offs among communication and sensing for the problem (11). Inspired by the idea from (Lin et al. 2019; Liu, Gu, and Zhang 2014), we decompose the problem (11) into several subproblems. Each subproblem emphasizes different preferences among two objectives, and these subproblems can be solved in parallel. To facilitate this decomposition, we define K unit vectors $\boldsymbol{u}_1, ..., \boldsymbol{u}_K \in \mathbb{R}^2_+$, and thus $\mathbb{R}^2_+$ is divided into K cones $\Omega_1, ..., \Omega_K$ given by

$$\Omega_k = \left\{\boldsymbol{q} \in \mathbb{R}^2_+ \mid \boldsymbol{u}_k^T\boldsymbol{q} \ge \boldsymbol{u}_j^T\boldsymbol{q}, \forall j = 1, ..., K\right\} \tag{12}$$

In other words, a vector $\boldsymbol{q}$ belongs to Ω_k if and only if $\boldsymbol{q}$ has the smallest angle to $\boldsymbol{u}_k$ among all the K preference vectors. Based on this division, the problem (11) can be decomposed into K subproblems. Subproblem k is given by

$$\begin{aligned} \min_{\boldsymbol{\gamma}} \quad & \boldsymbol{F}(\boldsymbol{\gamma}, \boldsymbol{\delta}) = [-\text{WSR}(\boldsymbol{\gamma}, \boldsymbol{\delta}), \text{CRLB}(\boldsymbol{\gamma})]^T \\ \text{s.t.} \quad & (\boldsymbol{u}_j - \boldsymbol{u}_k)^T(\boldsymbol{F}(\boldsymbol{\gamma}, \boldsymbol{\delta}) - \boldsymbol{e}) \le 0, \forall j = 1, \ldots, K \\ & \textstyle\sum_{i\in\mathcal{K}_l} ||\boldsymbol{v}_{l,i}||^2 + \text{Tr}(\boldsymbol{Q}_{l,0}) \le P_l, \quad \forall l \\ & \boldsymbol{\delta} = \arg\min_{\boldsymbol{\delta}'} \text{WSR}(\boldsymbol{\gamma}, \boldsymbol{\delta}') \\ & \quad \text{s.t.} \quad \|\boldsymbol{\Delta}'_{l,c,k}\|_2 \le \epsilon_{l,c,k}, \quad \forall l, c, k, \end{aligned} \tag{13}$$

where e_1 and e_2 are the lower bounds of $-\text{WSR}(\boldsymbol{\gamma}, \boldsymbol{\delta})$ and $\text{CRLB}(\boldsymbol{\gamma})$, respectively. The illustration in Appendix Figure 6 demonstrates how preference vectors partition the objective space into various subregions. Each solution to the subproblem is influenced by its associated preference vector, leading it towards a specific subregion.

To solve the subproblem (13), we first transform the lower-level problem into a constraint to the upper-level problem, and thus derive a single-level problem, which is a bi-objective optimization problem. Let $\phi(\boldsymbol{\gamma}) = \arg\min_{\boldsymbol{\delta}'}\{\text{WSR}\left(\boldsymbol{\gamma}, \boldsymbol{\delta}'\right) \mid \|\boldsymbol{\Delta}'_{l,c,k}\|_2 \le \epsilon_{l,c,k}, \forall l, c, k\}$ and $g(\boldsymbol{\gamma}, \boldsymbol{\delta}) = \|\boldsymbol{\delta} - \phi(\boldsymbol{\gamma})\|_2^2$, the problem (13) can be reformulated as a single-level problem

$$\begin{aligned} \min_{\boldsymbol{\gamma}, \boldsymbol{\delta}} \quad & \boldsymbol{F}(\boldsymbol{\gamma}, \boldsymbol{\delta}) = [-\text{WSR}(\boldsymbol{\gamma}, \boldsymbol{\delta}), \text{CRLB}(\boldsymbol{\gamma})]^T \\ \text{s.t.} \quad & r_j(\boldsymbol{\gamma}, \boldsymbol{\delta}) = (\boldsymbol{u}_j - \boldsymbol{u}_k)^T(\boldsymbol{F}(\boldsymbol{\gamma}, \boldsymbol{\delta}) - \boldsymbol{e}) \le 0, \forall j \\ & p_l(\boldsymbol{\gamma}) = \textstyle\sum_{i\in\mathcal{K}_l} ||\boldsymbol{v}_{l,i}||^2 + \text{Tr}(\boldsymbol{Q}_{l,0}) \le P_l, \quad \forall l \\ & g(\boldsymbol{\gamma}, \boldsymbol{\delta}) = 0. \end{aligned} \tag{14}$$

Following existing works on bilevel problems, an estimate of $\phi(\boldsymbol{\gamma})$ is enough instead of the exact $\phi(\boldsymbol{\gamma})$. Given that the lower-level problem is a constrained optimization problem, the augmented Lagrangian method is adopted. Considering the first-order Taylor approximation of $\text{WSR}(\boldsymbol{\gamma}, \boldsymbol{\delta}')$ with respect to $\boldsymbol{\gamma}$, i.e., for a given point $\bar{\boldsymbol{\gamma}}$, $\widetilde{\text{WSR}}(\boldsymbol{\gamma}, \boldsymbol{\delta}') = \text{WSR}(\bar{\boldsymbol{\gamma}}, \boldsymbol{\delta}') + \nabla_{\boldsymbol{\gamma}}\text{WSR}(\bar{\boldsymbol{\gamma}}, \boldsymbol{\delta}')^T(\boldsymbol{\gamma} - \bar{\boldsymbol{\gamma}})$, we rewrite the lower-level problem by introducing slack variables $\{\zeta_{l,c,k}\}$ as follows

$$\begin{aligned} \arg\min_{\boldsymbol{\delta}', \{\zeta_{l,c,k}\}} \quad & \widetilde{\text{WSR}}(\boldsymbol{\gamma}, \boldsymbol{\delta}') \\ \text{s.t.} \quad & \|\boldsymbol{\Delta}'_{l,c,k}\|_2 + \zeta_{l,c,k}^2 = \epsilon_{l,c,k}, \quad \forall l, c, k. \end{aligned} \tag{15}$$

Problem (15) can be solved through the augmented Lagrangian method. Thus, $\phi(\boldsymbol{\gamma})$ can be approximated after

K_{GD} steps of gradient descent which can be expressed as

$$\phi(\boldsymbol{\gamma}) = \boldsymbol{\delta}_0' - \sum_{k=0}^{K_{GD}-1} \eta_{\boldsymbol{\delta}'} \nabla_{\boldsymbol{\delta}'} f_{\text{ALM}k}, \tag{16}$$

where $f_{\text{ALM}k}$ represents the augmented Lagrangian function of the lower-level optimization problem (15). The relaxed problem of (14) is considered as

$$\begin{aligned} \min_{\boldsymbol{\gamma},\boldsymbol{\delta}} \quad & \boldsymbol{F}(\boldsymbol{\gamma},\boldsymbol{\delta}) = [-\text{WSR}(\boldsymbol{\gamma},\boldsymbol{\delta}), \text{CRLB}(\boldsymbol{\gamma})]^T \\ \text{s.t.} \quad & r_j(\boldsymbol{\gamma},\boldsymbol{\delta}) = (\boldsymbol{u}_j - \boldsymbol{u}_k)^T(\boldsymbol{F}(\boldsymbol{\gamma},\boldsymbol{\delta}) - \boldsymbol{e}) \le 0, \forall j \\ & p_l(\boldsymbol{\gamma}) = \textstyle\sum_{i\in\mathcal{K}_l} ||\boldsymbol{v}_{l,i}||^2 + \text{Tr}(\boldsymbol{Q}_{l,0}) \le P_l, \quad \forall l \\ & g(\boldsymbol{\gamma},\boldsymbol{\delta}) \le \varepsilon, \end{aligned} \tag{17}$$

where ε is a very small positive constant.

Theorem 1. *The function $g(\boldsymbol{\gamma},\boldsymbol{\delta})$ is convex with respect to $(\boldsymbol{\gamma},\boldsymbol{\delta})$ when $K_{GD} = 1$, and thus the feasible region formed by this constraint is convex.*

Proof. See Appendix D. □

In this paper, we utilize a set of cutting plane constraints, i.e. linear constraints, to approximate the convex feasible region formed by $g(\boldsymbol{\gamma},\boldsymbol{\delta}) \le \varepsilon$. The induced polytope $\mathcal{P}$ can be expressed as follows

$$\mathcal{P} = \left\{ \boldsymbol{a}_i^T\boldsymbol{\gamma} + \boldsymbol{b}_i^T\boldsymbol{\delta} + \kappa_i \le 0, i = 1, ..., |\mathcal{P}| \right\}, \tag{18}$$

where $\boldsymbol{a}_i$, $\boldsymbol{b}_i$ and κ_i are parameters in the i-th cutting plane and $|\mathcal{P}|$ denotes the number of cutting planes in $\mathcal{P}$. Thus, problem (17) can be written as

$$\begin{aligned} \min_{\boldsymbol{\gamma},\boldsymbol{\delta}} \quad & \boldsymbol{F}(\boldsymbol{\gamma},\boldsymbol{\delta}) = [-\text{WSR}(\boldsymbol{\gamma},\boldsymbol{\delta}), \text{CRLB}(\boldsymbol{\gamma})]^T \\ \text{s.t.} \quad & r_j(\boldsymbol{\gamma},\boldsymbol{\delta}) = (\boldsymbol{u}_j - \boldsymbol{u}_k)^T(\boldsymbol{F}(\boldsymbol{\gamma},\boldsymbol{\delta}) - \boldsymbol{e}) \le 0, \forall j \\ & p_l(\boldsymbol{\gamma}) = \textstyle\sum_{i\in\mathcal{K}_l} ||\boldsymbol{v}_{l,i}||^2 + \text{Tr}(\boldsymbol{Q}_{l,0}) \le P_l, \quad \forall l \\ & c_i(\boldsymbol{\gamma},\boldsymbol{\delta}) = \boldsymbol{a}_i^T\boldsymbol{\gamma} + \boldsymbol{b}_i^T\boldsymbol{\delta} + \kappa_i \le 0, \forall i = 1, ..., |\mathcal{P}^{[t]}|, \end{aligned} \tag{19}$$

where $\mathcal{P}^{[t]}$ is the polytope at t-th iteration. Now, we will commence the discussion on how cutting planes are updated during the iterations. The cutting planes will be updated every k_{pre} iterations based on the following two steps:

a) Removing inactive cutting planes. If $\boldsymbol{a}_i^T\boldsymbol{\gamma}^{[t+1]} + \boldsymbol{b}_i^T\boldsymbol{\delta}^{[t+1]} + \kappa_i < 0$, the i-th cutting plane will be removed.

b) Adding new cutting planes. Given a query point $(\boldsymbol{\gamma}^{[t+1]}, \boldsymbol{\delta}^{[t+1]})$, we check whether this point satisfies the constraint $g(\boldsymbol{\gamma},\boldsymbol{\delta}) \le \varepsilon$. If not, that is $g(\boldsymbol{\gamma},\boldsymbol{\delta}) > \varepsilon$, a valid cutting plane can be generated according to (Boyd and Vandenberghe 2007; Chen, Xiong, and Yang 2024) as follows

$$\begin{aligned} & g\left(\boldsymbol{\gamma}^{[t+1]}, \boldsymbol{\delta}^{[t+1]}\right) + \\ & \begin{bmatrix} \frac{\partial g\left(\boldsymbol{\gamma}^{[t+1]}, \boldsymbol{\delta}^{[t+1]}\right)}{\partial \boldsymbol{\gamma}} \\ \frac{\partial g\left(\boldsymbol{\gamma}^{[t+1]}, \boldsymbol{\delta}^{[t+1]}\right)}{\partial \boldsymbol{\delta}} \end{bmatrix}^T \left(\begin{bmatrix} \boldsymbol{\gamma} \\ \boldsymbol{\delta} \end{bmatrix} - \begin{bmatrix} \boldsymbol{\gamma}^{[t+1]} \\ \boldsymbol{\delta}^{[t+1]} \end{bmatrix} \right) \le \varepsilon. \end{aligned} \tag{20}$$

For the constrained bi-objective subproblem (19), our goal is to achieve Pareto critical optimality.

Algorithm 1: BOBLRBF: Bi-Objective BiLevel optimization based Robust BeamForming.

Input: $\boldsymbol{P}$, $\left\{\widetilde{\boldsymbol{h}}_{l,c,k}, \epsilon_{l,c,k}, \boldsymbol{H}_{l,j,m}\right\}$, a set of preference vectors $\{\boldsymbol{u}_1, \boldsymbol{u}_2, ..., \boldsymbol{u}_K\}$.
Output: The set of solutions $\{\boldsymbol{\gamma}_k, \boldsymbol{\delta}_k\}_k$.
(can be solved in parallel)
for $k = 1$ **to** K **do**
  Initialization: set $t_k = 0$, $\boldsymbol{\gamma}_k^{[0]}$ within power budgets, $\boldsymbol{\delta}_k^{[0]} = 0$;
  repeat
    Find the direction $\boldsymbol{d}_k^{[t]}$ by solving problem (22);
    Update variables $\boldsymbol{\gamma}_k^{[t+1]}$ and $\boldsymbol{\delta}_k^{[t+1]}$ based on (23);
    if t_k mod $k_{pre} == 0$ **then**
      Remove inactive cutting planes;
      Compute an estimate solution $\phi(\boldsymbol{\gamma}_k^{[t+1]})$ of the lower level problem according to (16);
      if $g(\boldsymbol{\gamma}_k^{[t+1]}, \boldsymbol{\delta}_k^{[t+1]}) > \varepsilon$ **then**
        Add the new cutting plane according to (20);
      end if
    end if
    $t_k \leftarrow t_k + 1$;
  until convergence.
end for

Definition 1. *(Locally Pareto optimality) A feasible solution $(\boldsymbol{\gamma},\boldsymbol{\delta})$ is locally Pareto optimal if there is a neighborhood U of $(\boldsymbol{\gamma},\boldsymbol{\delta})$ such that there does not exist a feasible point $(\boldsymbol{\gamma}',\boldsymbol{\delta}') \in U$ with $\boldsymbol{F}(\boldsymbol{\gamma}',\boldsymbol{\delta}') \preceq \boldsymbol{F}(\boldsymbol{\gamma},\boldsymbol{\delta})$ and $F_i(\boldsymbol{\gamma}',\boldsymbol{\delta}') < F_i(\boldsymbol{\gamma},\boldsymbol{\delta})$ for at least one index i.*

Definition 2. *(Pareto critical point) A necessary condition for a feasible point $(\boldsymbol{\gamma},\boldsymbol{\delta})$ to be Pareto critical point is*

$$range(J\boldsymbol{F}(\boldsymbol{\gamma},\boldsymbol{\delta})) \cap (-\mathbb{R}_{++}) = \emptyset, \tag{21}$$

where $J\boldsymbol{F}(\boldsymbol{\gamma},\boldsymbol{\delta})$ denotes the Jacobian of $\boldsymbol{F}$ at $(\boldsymbol{\gamma},\boldsymbol{\delta})$.

We denote the set of active constraints at a feasible point $(\bar{\boldsymbol{\gamma}},\bar{\boldsymbol{\delta}})$ by $I_r(\bar{\boldsymbol{\gamma}},\bar{\boldsymbol{\delta}})$, $I_p(\bar{\boldsymbol{\gamma}},\bar{\boldsymbol{\delta}})$ and $I_c(\bar{\boldsymbol{\gamma}},\bar{\boldsymbol{\delta}})$. $I_r(\bar{\boldsymbol{\gamma}},\bar{\boldsymbol{\delta}})$ is given by $I_r(\bar{\boldsymbol{\gamma}},\bar{\boldsymbol{\delta}}) = \{j | r_j(\bar{\boldsymbol{\gamma}},\bar{\boldsymbol{\delta}}) \ge 0\}$, with $I_p(\bar{\boldsymbol{\gamma}},\bar{\boldsymbol{\delta}})$ and $I_c(\bar{\boldsymbol{\gamma}},\bar{\boldsymbol{\delta}})$ being defined in the same way. We can find a descent direction for problem (19) by solving a quadratic programming problem

$$\begin{aligned} \arg\min_{\boldsymbol{d},\varphi} \quad & \varphi + \tfrac{1}{2}\|\boldsymbol{d}\|^2 \\ \text{s.t.} \quad & \nabla F_k(\boldsymbol{\gamma}^{[t]},\boldsymbol{\delta}^{[t]})^T\boldsymbol{d} \le \varphi, \quad \forall k = 1, 2 \\ & \nabla r_j(\boldsymbol{\gamma}^{[t]},\boldsymbol{\delta}^{[t]})^T\boldsymbol{d} \le \varphi, \quad \forall j \in I_r(\boldsymbol{\gamma}^{[t]},\boldsymbol{\delta}^{[t]}) \\ & \nabla p_l(\boldsymbol{\gamma}^{[t]},\boldsymbol{\delta}^{[t]})^T\boldsymbol{d} \le \varphi, \quad \forall l \in I_p(\boldsymbol{\gamma}^{[t]},\boldsymbol{\delta}^{[t]}) \\ & \nabla c_i(\boldsymbol{\gamma}^{[t]},\boldsymbol{\delta}^{[t]})^T\boldsymbol{d} \le \varphi, \quad \forall i \in I_c(\boldsymbol{\gamma}^{[t]},\boldsymbol{\delta}^{[t]}). \end{aligned} \tag{22}$$

Lemma 1. *Let $\left(\boldsymbol{d}^{[t]}, \varphi^{[t]}\right)$ be the solution of problem (22).*

1. *If $\left(\boldsymbol{\gamma}^{[t]}, \boldsymbol{\delta}^{[t]}\right)$ is the Pareto critical point, then $\boldsymbol{d}^{[t]} = \boldsymbol{0}$ and $\varphi^{[t]} = 0$.*

2. *If* $\left(\boldsymbol{\gamma}^{[t]}, \boldsymbol{\delta}^{[t]}\right)$ *is not the Pareto critical point, then* $\varphi^{[t]} \leq -\frac{1}{2}\|\boldsymbol{d}^{[t]}\|^2 < 0$.

Proof. See Appendix E. □

We can obtain a Pareto critical solution for each subproblem by iteratively updating variables as follows

$$(\boldsymbol{\gamma}^{[t+1]}, \boldsymbol{\delta}^{[t+1]}) = (\boldsymbol{\gamma}^{[t]}, \boldsymbol{\delta}^{[t]}) + \eta^{[t]}\boldsymbol{d}^{[t]}, \tag{23}$$

where $\eta^{[t]}$ represents the stepsize as the maximum of

$$\begin{aligned}\{\eta = &\frac{1}{2^j} \,|\, j \in \mathbb{N}, \boldsymbol{F}((\boldsymbol{\gamma}^{[t]}, \boldsymbol{\delta}^{[t]}) + \eta\boldsymbol{d}^k) \preceq \\ &\boldsymbol{F}(\boldsymbol{\gamma}^{[t]}, \boldsymbol{\delta}^{[t]}) + \varsigma\eta J\boldsymbol{F}(\boldsymbol{\gamma}^{[t]}, \boldsymbol{\delta}^{[t]})\boldsymbol{d}^{[t]}\},\end{aligned} \tag{24}$$

where $\varsigma \in [0, 1]$ is a prespecified constant.

The details of BOBLRBF are summarized in Algorithm 1.

Assumption 1. *We assume that* $\boldsymbol{F}_i$ *has Lipschitz continuous gradients, i.e., for any* $(\boldsymbol{\gamma}, \boldsymbol{\delta})$, $(\boldsymbol{\gamma}', \boldsymbol{\delta}')$, *we assume that there exists* $L_i > 0$ *satisfying that*

$$\|\nabla\boldsymbol{F}_i(\boldsymbol{\gamma}, \boldsymbol{\delta}) - \nabla\boldsymbol{F}_i(\boldsymbol{\gamma}', \boldsymbol{\delta}')\| \leq L_i\|(\boldsymbol{\gamma}, \boldsymbol{\delta}) - (\boldsymbol{\gamma}', \boldsymbol{\delta}')\| \tag{25}$$

Theorem 2. *The Algorithm 1 has a convergence rate of* $\mathcal{O}(\frac{1}{\sqrt{T}})$, *where* T *is the iteration numbers of Algorithm 1.*

Proof. See Appendix F. □

GPU-Accelerated Bilevel Optimization

In this section, we design an interpretable neural network architecture BOBLRBF-DNN inspired by the convergent optimization algorithm BOBLRBF, as shown in Figure 2. Traditional optimization algorithms generally demand a substantially smaller number of parameters in comparison to widely used neural networks. This inherent efficiency renders optimization algorithm-inspired neural networks highly parameter-efficient, necessitating less training data. Additionally, BOBLRBF-DNN naturally inherits prior structures, as opposed to learning from scratch through extensive training data. Consequently, BOBLRBF-DNN often exhibits superior generalization capabilities and can be computationally faster compared to generic neural networks.

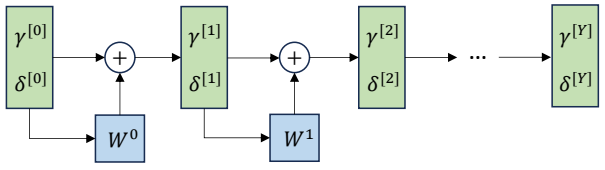

Figure 2: The neural network architecture of our BOBLRBF-DNN.

Specifically, we unroll the algorithm BOBLRBF and use a neural network to approximate the descent direction $\boldsymbol{d}^{[t]}$ in (23). In other words, there is no need to solve the quadratic programming problem (22). Instead, the aim is to enable the neural network to learn the gradient information required for the variable updates in the BOBLRBF algorithm. We have

$$(\boldsymbol{\gamma}^{[y+1]}, \boldsymbol{\delta}^{[y+1]}) = (\boldsymbol{\gamma}^{[y]}, \boldsymbol{\delta}^{[y]}) + \eta^{[y]}W^y(\boldsymbol{w}^y; \boldsymbol{\gamma}^{[y]}, \boldsymbol{\delta}^{[y]}), \tag{26}$$

where W^y can be any neural network parameterized by $\boldsymbol{w}^y$.

Note that the parameter $\boldsymbol{w}^y$ varies from layer to layer, rather than being shared across different layers. This design is intended to provide distinct model parameters at each iteration of the optimization algorithm, which can enhance the performance of the model. Interestingly, the inspired neural network architecture by this approach bears a striking resemblance to ResNet.

The cutting planes are updated based on $(\boldsymbol{\gamma}^{[Y]}, \boldsymbol{\delta}^{[Y]})$ like Algorithm 1. After a certain number of iterations, the cutting planes will be fixed. Based on the penalty function method and problem (19), the loss function is defined as

$$\begin{aligned}&loss(\boldsymbol{w}) = \tfrac{1}{M}\textstyle\sum_{m=1}^{M} loss^{(m)}(\boldsymbol{w}; \boldsymbol{\gamma}^{[Y](m)}, \boldsymbol{\delta}^{[Y](m)}) \\ &= \tfrac{1}{M}\textstyle\sum_{m=1}^{M} -\lambda_1\mathrm{WSR}^{(m)} + \lambda_2\mathrm{CRLB}^{(m)} \\ &+ \textstyle\sum_l \sigma_l \max\{0, p_l^{(m)} - P_l^{(m)}\}^2 + \sum_i \sigma_i \max\{0, c_i^{(m)}\}^2,\end{aligned} \tag{27}$$

where $\boldsymbol{w} = (\boldsymbol{w}^0, \ldots, \boldsymbol{w}^{Y-1})$, and M is the number of samples. λ_1 and λ_2 are weighting factors. $\{\sigma_l\}$ and $\{\sigma_i\}$ are increasing penalty parameters. We can find that one forward propagation is equivalent to iterating Algorithm 1 Y times.

Experiments

This section provides numerical experiments to validate the performance of our proposed BOBLRBF and BOBLRBF-DNN. The algorithm BOBLRBF is executed on a machine equipped with 12th Gen Intel(R) Core(TM) i7-12700H and the algorithm BOBLRBF-DNN runs on NVIDIA GeForce RTX 3060. All experimental results are averaged over multiple runs.

In the simulation, we consider the networked ISAC scenario with $L = 3$ BSs. BSs are deployed with uniform linear arrays (ULAs) with half-wavelength spacing between consecutive antennas, and each BS serves one communication user. The number of antennas at each BS is $N = 5$. BSs are located at $(-40\mathrm{m}, 40\sqrt{3}\mathrm{m})$, $(80\mathrm{m}, 0\mathrm{m})$ and $(-40\mathrm{m}, -40\sqrt{3}\mathrm{m})$, respectively, while communication users are randomly distributed around BSs. There are $J = 2$ targets located at $(2\mathrm{m}, 5\mathrm{m})$ and $(-5\mathrm{m}, 1\mathrm{m})$. The communication channels between BSs and communication users are set as Rayleigh fading following the standard assumption, i.e., each channel coefficient $\boldsymbol{h}_{l,c,k}$ is generated according to a complex standard normal distribution, with zero mean and unit variance. Furthermore, the path loss between each BS and the communication user is given by $\mathrm{PL}_{l,c,k} = \rho(\frac{d_0}{d_{l,c,k}})^\nu$, where ρ represents the path loss at the reference distance of $d_0 = 1\mathrm{m}$ and ν denotes the path loss exponent.

First, we verify the performance of the BOBLRBF algorithm under the presence of channel estimation errors as shown in Figure 3. The power budgets $\{P_l\}$ of all BSs are set to be 40 dBm. Our proposed algorithm BOBLRBF exhibits the capability to generate a set of well-representative

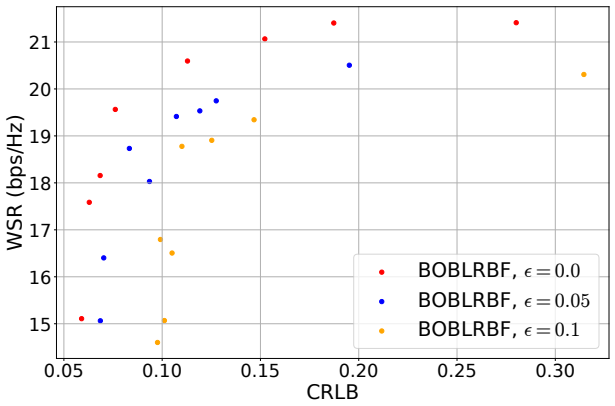

Figure 3: The WSR versus the CRLB in the case with $L = 3$, $J = 2$ and $K_i = 1, i = 1, 2, 3$ for different uncertainty regions of CSI.

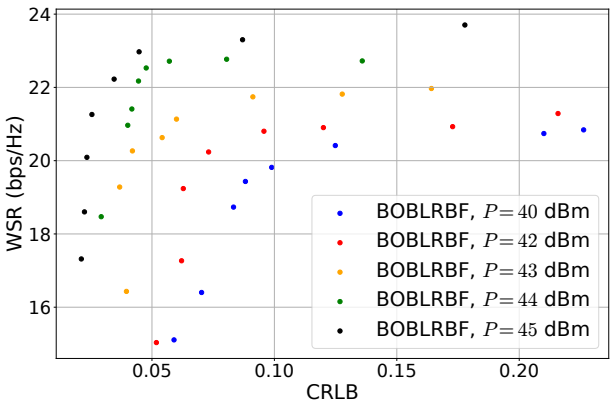

Figure 4: The WSR versus the CRLB in the case with $L = 3$, $J = 2$ and $K_i = 1, i = 1, 2, 3$ for different power budgets.

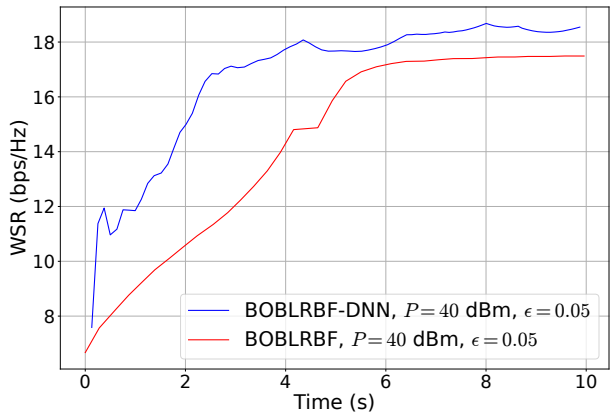

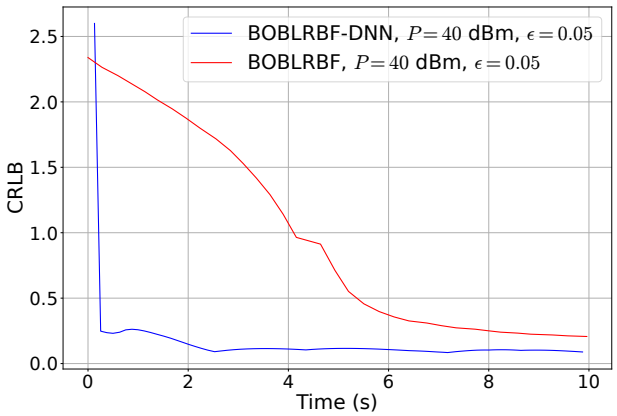

Figure 5: Comparing the convergence rate of our proposed BOBLRBF and BOBLRBF-DNN.

solutions with different trade-offs among communication and localization performance. Additionally, We can observe that when uncertainty regions of CSI become larger, both communication and localization performances will decrease slightly. This is primarily because larger regions of uncertainty indicate more significant channel estimation errors, which consequently lead to a reduced worst-case WSR and CRLB.

Then, we begin to explore the impact of power on communication and sensing performance in the presence of CSI errors. As depicted in Figure 4, an increase in the power budget $\boldsymbol{P}$ correlates with improvements in both communication and sensing performances. This observation aligns with the anticipated outcomes within ISAC systems.

Finally, we illustrate the disparity in convergence rates between our proposed BOBLRBF and BOBLRBF-DNN algorithms in Figure 5. In experiments, we set $W^y, y = 1, \ldots, Y - 1$ as multilayer perceptrons (MLPs). It is evident that the BOBLRBF-DNN method exhibits a more rapid convergence and achieves better communication and localization performances than the BOBLRBF algorithm. This is attributed to the parallel computing capabilities of GPUs. Moreover, we find that with the BOBLRBF-DNN architecture, the CRLB becomes very small in a relatively short time, indicating that the system achieves excellent sensing performance quickly.

Conclusion

We propose to model robust ISAC systems from the perspective of GPU-accelerated bilevel optimization. This paper studies a practical ISAC system in the presence of CSI errors. An efficient iterative algorithm, named BOBLRBF, is proposed to address this challenging hierarchical problem with two objectives. We also provide a theoretical analysis regarding the convergence rate. Furthermore, we design an accelerated bilevel optimization algorithm that can be implemented via GPU in parallel. Numerical results are provided to confirm our algorithm BOBLRBF can generate a diverse array of Pareto critical solutions, effectively balancing the trade-offs between communication efficiency and sensing precision. We also show that the BOBLRBF-DNN algorithm exhibits a faster convergence rate compared to the BOBLRBF algorithm, achieving up to a 50-fold acceleration in convergence speed during the experiments.

Acknowledgments

This work was supported in part by the National Natural Science Foundation of China under Grant 12371519 and 61771013; in part by Asiainfo Technologies; in part by the Fundamental Research Funds for the Central Universities of China; and in part by the Fundamental Research Funds of Shanghai Jiading District.

References

Adler, J.; and Öktem, O. 2018. Learned primal-dual reconstruction. *IEEE Transactions on Medical Imaging*, 37(6): 1322–1332.

Boyd, S.; and Vandenberghe, L. 2007. Localization and cutting-plane methods. *From Stanford EE 364b lecture notes*, 386.

Camacho-Vallejo, J.-F.; López-Vera, L.; Smith, A. E.; and González-Velarde, J.-L. 2022. A tabu search algorithm to solve a green logistics bi-objective bi-level problem. *Annals of Operations Research*, 316(2): 927–953.

Cao, N.; Chen, Y.; Gu, X.; and Feng, W. 2020. Joint bi-static radar and communications designs for intelligent transportation. *IEEE Transactions on Vehicular Technology*, 69(11): 13060–13071.

Chen, W.; and Kwok, J. 2022a. Multi-objective deep learning with adaptive reference vectors. In *Advances in Neural Information Processing Systems*, volume 35, 32723–32735.

Chen, W.; and Kwok, J. 2022b. Multi-objective deep learning with adaptive reference vectors. In *Advances in Neural Information Processing Systems*, volume 35, 32723–32735.

Chen, X.; Xiong, Y.; and Yang, K. 2024. Robust beamforming for downlink multi-cell cystems: A bilevel optimization perspective. In *Proceedings of the AAAI Conference on Artificial Intelligence*, volume 38, 7969–7977.

Chen, Y.; and Gu, X. 2021. Time allocation for integrated bi-static radar and communication systems. *IEEE Communications Letters*, 25(3): 1033–1036.

Cheng, G.; Fang, Y.; Xu, J.; and Ng, D. W. K. 2024. Optimal coordinated transmit beamforming for networked integrated sensing and communications. *IEEE Transactions on Wireless Communications*, 1–1.

Demirhan, U.; and Alkhateeb, A. 2023. Cell-free ISAC MIMO systems: Joint sensing and communication beamforming. *arXiv preprint arXiv:2301.11328*.

Fliege, J.; and Svaiter, B. F. 2000. Steepest descent methods for multicriteria optimization. *Mathematical methods of operations research*, 51: 479–494.

Franceschi, L.; Frasconi, P.; Salzo, S.; Grazzi, R.; and Pontil, M. 2018. Bilevel programming for hyperparameter optimization and meta-learning. In *International conference on machine learning*, 1568–1577. PMLR.

Godrich, H.; Haimovich, A. M.; and Blum, R. S. 2010. Target localization accuracy gain in MIMO radar-based systems. *IEEE Transactions on Information Theory*, 56(6): 2783–2803.

Gregor, K.; and LeCun, Y. 2010. Learning fast approximations of sparse coding. In *Proceedings of the 27th International Conference on International Conference on Machine Learning*, ICML'10, 399–406. Madison, WI, USA: Omnipress. ISBN 9781605589077.

Gutjahr, W. J.; and Dzubur, N. 2016. Bi-objective bilevel optimization of distribution center locations considering user equilibria. *Transportation Research Part E: Logistics and Transportation Review*, 85: 1–22.

Hong, M.; Wai, H.-T.; Wang, Z.; and Yang, Z. 2023. A two-timescale framework for bilevel optimization: Complexity analysis and application to actor-critic. *SIAM Journal on Optimization*, 33(1): 147–180.

Hua, H.; Xu, J.; and Han, T. X. 2023. Optimal transmit beamforming for integrated sensing and communication. *IEEE Transactions on Vehicular Technology*, 72(8): 10588–10603.

Huang, Y.; Fang, Y.; Li, X.; and Xu, J. 2022. Coordinated power control for network integrated sensing and communication. *IEEE Transactions on Vehicular Technology*, 71(12): 13361–13365.

Ji, K.; Lee, J. D.; Liang, Y.; and Poor, H. V. 2020. Convergence of meta-learning with task-specific adaptation over partial parameters. In *Advances in Neural Information Processing Systems*, 11490–11500.

Ji, K.; Yang, J.; and Liang, Y. 2021. Bilevel optimization: Convergence analysis and enhanced design. In *International conference on machine learning*, 4882–4892. PMLR.

Jiao, Y.; Yang, K.; Wu, T.; Jian, C.; and Huang, J. 2024. Provably convergent federated trilevel learning. In *Proceedings of the AAAI Conference on Artificial Intelligence*, volume 38, 12928–12937.

Jiao, Y.; Yang, K.; Wu, T.; Song, D.; and Jian, C. 2023. Asynchronous distributed bilevel optimization. In *International Conference on Learning Representations*.

Kim, I. Y.; and De Weck, O. L. 2005. Adaptive weighted-sum method for bi-objective optimization: Pareto front generation. *Structural and multidisciplinary optimization*, 29: 149–158.

Li, Y.; Tofighi, M.; Monga, V.; and Eldar, Y. C. 2019. An algorithm unrolling approach to deep image deblurring. In *ICASSP 2019 - 2019 IEEE International Conference on Acoustics, Speech and Signal Processing (ICASSP)*, 7675–7679.

Lin, X.; Zhen, H.-L.; Li, Z.; Zhang, Q.-F.; and Kwong, S. 2019. Pareto multi-task learning. In *Advances in Neural Information Processing Systems*, volume 32. Curran Associates, Inc.

Liu, F.; Cui, Y.; Masouros, C.; Xu, J.; Han, T. X.; Eldar, Y. C.; and Buzzi, S. 2022a. Integrated sensing and communications: Toward dual-functional wireless networks for 6G and beyond. *IEEE Journal on Selected Areas in Communications*, 40(6): 1728–1767.

Liu, F.; Liu, Y.-F.; Li, A.; Masouros, C.; and Eldar, Y. C. 2022b. Cramér-Rao bound optimization for joint radar-communication beamforming. *IEEE Transactions on Signal Processing*, 70: 240–253.

Liu, F.; Masouros, C.; Li, A.; Ratnarajah, T.; and Zhou, J. 2018. MIMO radar and cellular coexistence: A power-efficient approach enabled by interference exploitation. *IEEE Transactions on Signal Processing*, 66(14): 3681–3695.

Liu, H.; Simonyan, K.; and Yang, Y. 2018. Darts: Differentiable architecture search. In *International Conference on Learning Representations*.

Liu, H.-L.; Gu, F.; and Zhang, Q. 2014. Decomposition of a multiobjective optimization problem into a number of simple multiobjective subproblems. *IEEE Transactions on Evolutionary Computation*, 18(3): 450–455.

Liu, R.; Liu, X.; Yuan, X.; Zeng, S.; and Zhang, J. 2021. A value-function-based interior-point method for non-convex bi-level optimization. In *International Conference on Machine Learning*, 6882–6892. PMLR.

Liu, X.; Huang, T.; Shlezinger, N.; Liu, Y.; Zhou, J.; and Eldar, Y. C. 2020. Joint transmit beamforming for multiuser MIMO communications and MIMO radar. *IEEE Transactions on Signal Processing*, 68: 3929–3944.

Tajer, A.; Prasad, N.; and Wang, X. 2011. Robust linear precoder design for multi-cell downlink transmission. *IEEE Transactions on Signal Processing*, 59(1): 235–251.

Wang, S.; Dai, W.; Wang, H.; and Li, G. Y. 2024. Robust waveform design for integrated sensing and communication. *IEEE Transactions on Signal Processing*.

Wang, X.; Fei, Z.; Zhang, J. A.; Huang, J.; and Yuan, J. 2021. Constrained utility maximization in dual-functional radar-communication multi-UAV networks. *IEEE Transactions on Communications*, 69(4): 2660–2672.

Wu, Z.; Xiao, M.; Fang, C.; and Lin, Z. 2024. Designing universally-approximating deep neural networks: A first-order optimization approach. *IEEE Transactions on Pattern Analysis and Machine Intelligence*, 1–17.

Xu, Y.; Xu, D.; Xie, L.; and Song, S. 2023. Joint BS selection, user association, and beamforming design for network integrated sensing and communication. In *GLOBECOM 2023-2023 IEEE Global Communications Conference*, 3111–3117. IEEE.

Xue, C.; Wang, X.; Yan, J.; Hu, Y.; Yang, X.; and Sun, K. 2021. Rethinking bi-level optimization in neural architecture search: A gibbs sampling perspective. In *Proceedings of the AAAI Conference on Artificial Intelligence*, volume 35, 10551–10559.

Yang, K.; Huang, J.; Wu, Y.; Wang, X.; and Chiang, M. 2014. Distributed robust optimization (DRO), part I: Framework and example. *Optimization and Engineering*, 15(1): 35–67.

Yang, K.; Wu, Y.; Huang, J.; Wang, X.; and Verdú, S. 2008. Distributed robust optimization for communication networks. In *IEEE INFOCOM 2008-The 27th Conference on Computer Communications*, 1157–1165. IEEE.

Yang, Y.; Sun, J.; Li, H.; and Xu, Z. 2020. ADMM-CSNet: A deep learning approach for image compressive sensing. *IEEE Transactions on Pattern Analysis and Machine Intelligence*, 42(3): 521–538.

Ye, F.; Lin, B.; Cao, X.; Zhang, Y.; and Tsang, I. 2024. A first-order multi-gradient algorithm for multi-objective bi-level optimization. *arXiv preprint arXiv:2401.09257*.

YE, F.; Lin, B.; Yue, Z.; Guo, P.; Xiao, Q.; and Zhang, Y. 2021. Multi-objective meta learning. In *Advances in Neural Information Processing Systems*, volume 34, 21338–21351.

Yeung, D. W.; and Zhang, Y. 2023. Bi-objective optimization: A pareto method with analytical solutions. *Applied Mathematics*, 14(1): 57–81.

Zhang, H.; Zhang, H.; Di, B.; Renzo, M. D.; Han, Z.; Poor, H. V.; and Song, L. 2022a. Holographic integrated sensing and communication. *IEEE Journal on Selected Areas in Communications*, 40(7): 2114–2130.

Zhang, J. A.; Rahman, M. L.; Wu, K.; Huang, X.; Guo, Y. J.; Chen, S.; and Yuan, J. 2022b. Enabling joint communication and radar sensing in mobile networks—A survey. *IEEE Communications Surveys & Tutorials*, 24(1): 306–345.